Role of one-dimensional defects in the electrical transport through Si(111)-7 × 7 surface states

Masayuki Hamada and Yukio Hasegawa
The Institute for Solid State Physics, The University of Tokyo, 5-1-5 Kashiwa-no-ha, Kashiwa 277-8581, Japan

(Received 21 September 2018; revised manuscript received 4 February 2019; published 4 March 2019)

Using scanning tunneling potentiometry, we have obtained spatial distribution of electrochemical potential on the Si(111)-7 × 7 surface and estimated a ratio of conductance across surface steps and domain boundaries to that of the reconstructed terrace. Our measurements reveal significant resistance across the steps, indicating that the conductance on the 7 × 7 surface measured in macroscopic methods is basically determined by the step density, which is uncontrolled in most of the macroscopic measurements. The domain boundaries also exhibit measurable resistance, implying underestimation (overestimation) of the 7 × 7 terrace (step) conductance when these conductance values are estimated from the anisotropy in the conductance along and across the step directions without considering the resistance at the domain boundaries.

DOI: 10.1103/PhysRevB.99.125402

I. INTRODUCTION

Atomically thin two-dimensional electron systems (2DESs), which can be found in graphene [1], transition-metal dichalcogenides [2,3], etc., have been one of the hot topics in condensed-matter physics because of their unique properties originating from the low dimensionality and reduced symmetry. Among them, 2DESs with metallic surface states, which are formed by a few-monolayer deposition of metallic elements on semiconducting substrates, have a unique status. Because of the thermal stability through the surface atomic reconstruction, high-quality self-organized samples can be formed in macroscopic dimensions. Basic properties such as atomic structure and electronic states are well characterized by standard surface science techniques including scanning tunneling microscopy (STM). The carrier density can also be controlled by depositing adsorbates on it [4–6].

Recently 2DESs with metallic surface states attracted further attention because of the discovery of superconductivity [7]. Since then many research works have been devoted to understanding transport properties through the states. Four-probe methods, in which electrode spacing goes down to the micrometer level in order to improve the surface sensitivity [8–10], have been utilized for the conductance measurement through the states [10–12]. Methods of measuring local electrochemical potential by STM were also used to evaluate the conductivity through the states [12–15]. It has been, however, difficult to acquire intrinsic conductivity through the surface states, and in fact the measured conductance varies drastically by several orders depending on the methods. One of the reasons for the disagreement is the inevitable presence of local defects on the surfaces. Net and local misorientation of the surface from the nominally flat plane result in the formation of steps on the substrate. Superstructure due to the surface reconstruction inherently forms boundaries that separate domains the periodical phase of which does not match there. Both of the one-dimensional (1D) line defects disrupt the periodicity of the surface atomic arrangement and therefore work as a barrier for the Bloch electrons across them. Indeed, surface-conductance studies demonstrated significant resistances at monoatomic-height steps on metallic surface states [11,16]. The step resistivity explains why the conductance measured on single terraces using STM-based local probe methods [10–14,17] is different from the ones measured across the sample surface using macroscopic probes.

To further investigate the role of the line defects in the transport, we investigated the conductance of the 7 × 7 structure of Si(111) substrates, which has an archetypical metallic surface state. The conductance on the surface has been extensively investigated by several groups [13,18–22], but still debated, in particular, concerning the role of the resistance across steps to the total conductance. Actually, until quite recently the conductance across a single step of the surface had not been measured [10,12]. In the present paper, using a microscopic technique to measure a profile of local electrochemical potential or Fermi level, called scanning tunneling potentiometry (STP) [14,23–30], we investigate the potential profile across the line defects. STP is a powerful tool to investigate transport properties in atomic scale, and indeed has been utilized to elucidate the transport properties at various local structures including edges of graphene layers [27,29,30].

Using STP, we observed that the potential drops clearly at step edges and phase boundaries of the 7 × 7 reconstructed surface, indicating the presence of significant electrical resistance there. The step and terrace conductance has been characterized from the anisotropy in the conductance measured along and normal to the steps, assuming that the resistance measured across the steps arises from that of steps and terrace while the resistance along the steps is only due to the terrace. As the phase boundary tends to bridge the steps, the presence of resistance at phase boundaries should modify the transport along the step edges significantly, leading to underestimation (overestimation) in the intrinsic terrace (step) conductance. Our measurements emphasize the significance of the line defects in the net conductance and the necessity to characterize conductance microscopically in order to understand the intrinsic transport properties of the metallic surface states.

II. EXPERIMENTAL

In this paper we measured spatial distribution of the electrochemical potential over 7×7 surfaces that include steps and domain boundaries using STP in ultrahigh-vacuum (UHV) conditions at room temperature. In the UHV chamber a nominally (111)-oriented Si wafer (n type, 1000 Ω cm) was annealed via direct resistive heating to 1200 °C to form the 7×7 structure on the surface. For the STP measurements, the electrical current through the conductive layer, which is required to make a potential gradient, was introduced between two 2×2-mm^2 tantalum pads separated by 2 mm. The electrodes were deposited onto the surface by mask evaporation prior to the loading into the UHV chamber. We have taken both the STM image and the electrochemical potential mapping simultaneously [28]; the potential was measured from the bias voltage that nulls the tunneling current while the tip height was stabilized by setting differential tunneling conductance (dI/dV) at the nulled bias voltage constant. All the data presented in this paper were taken with the sample bias voltage modulated at 2.0 kHz with the amplitude of 5 mV. The modulated amplitude of the tunneling current was set at 20 pA for the STM feedback.

III. EXPERIMENTAL RESULTS

A. Step conductivity

Figure 1 shows STM and electrochemical potential images taken simultaneously on the 7×7 surface around the middle of the two Ta electrodes. The net current flows in the horizontal direction from the left to the right of the images. Bilayer-high (0.31 nm) steps are found from the upper left to the lower right in the topographic image [Fig. 1(a)] and its cross-sectional plot [upper panel of Fig. 1(c)]. Because of the presence of the high-density steps, the current distribution is strongly modified from the macroscopic one. The direction of the local current on the 7×7 terrace, which can be estimated from the gradient of the measured potential distribution, is severely tilted from the horizontal direction toward the direction along the steps. We found such deviation in the area where the terrace width is <200 nm. The observed tilted current clearly demonstrates that the steps are a strong resistive barrier for the electrons in the metallic surface states, as already stated in previous reports [10,12].

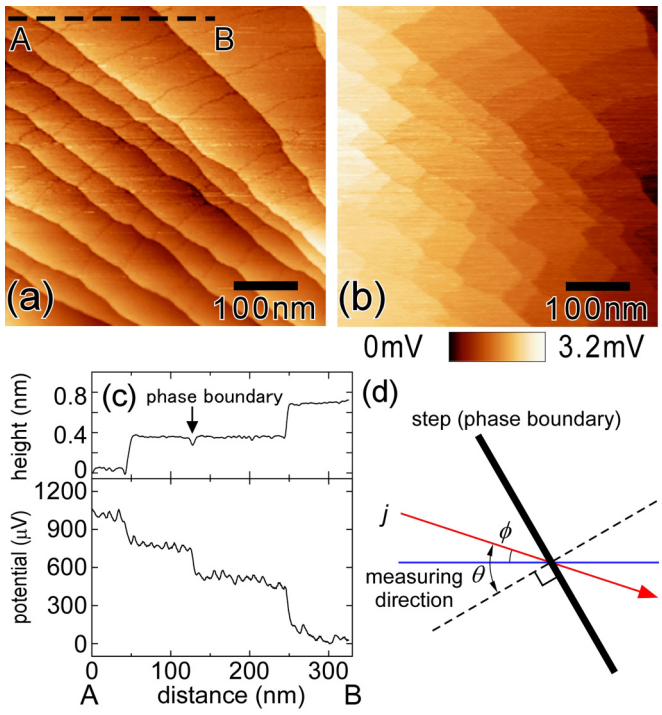

FIG. 1. STM (a) and electrochemical potential (b) images taken simultaneously on the Si(111)-7×7 surface. The applied voltage and net current flowing through the Ta pads are 9.5 V and 0.52 mA, respectively. (c) Cross-sectional plots of topographic height and potential taken along the dashed line drawn in panel (a). (d) Definition of the angles between the current flow, the measurement direction, and the direction normal to the step.

The steps are, however, not the only defects that disrupt the electron transport on the surface. In the potential mapping shown in Fig. 1(b), which exhibits a ladderlike pattern, one notices several potential drops in the narrow area between the steps. The potential drop due to the rungs of the ladders is more clearly displayed in a cross-sectional profile shown in Fig. 1(c), which was taken along the dashed line in Fig. 1(a). The rungs correspond to boundaries that separate domains of the 7×7 reconstructed structures the phases of which do not match. The reconstructed structures nucleate on the surface with 49 possible phases and the boundaries are formed where the phase-different domains meet. The potential profiles indicate that the phase boundaries also have electrical resistance.

From the obtained potential images and their cross-sectional plots, we can quantitatively analyze the conductivity through an individual step and phase boundary. In the configuration of the potentiometry, the conductivity σ [S/m] across a 1D line defect on surfaces (steps, phase boundaries, etc.) can be described as $\sigma = j \cos\theta / \Delta V$ with the potential drop ΔV [V] across the 1D defect. Here, j [A/m] is the current density across the defect and θ is an angle between the current flow direction and the direction normal to the line defect, as shown in Fig. 1(d). The direction of the local current flow can be estimated from the gradient of the measured potential on terraces. The amount of the local current density j is then also described with the potential gradient E [V/m] measured in the terraces nearby as $j = \sigma_t E / \cos\varphi$, where σ_t [S] is the conductivity of the 7×7 terrace and φ is the angle between the local current direction and the direction in which the potential gradient was measured [see Fig. 1(d)]. From the two equations, the ratio of the step (phase boundary) conductivity $\sigma_{s(pb)}$ to the terrace conductivity σ_t is described as $\sigma_{s(pb)}/\sigma_t = E \cos\theta / (\Delta V \cos\varphi)$. Since the absolute value of the current density, obviously different from the macroscopic current divided by the width of the Ta electrodes, is unknown, we cannot measure the terrace or phase boundary conductivity directly. But, their ratio can be estimated precisely through the analysis of the potential mappings.

In our measurement we used low-doped substrates, and therefore the electrical conductance through the substrate is expected to be quite small. But, there is a possibility that the substrate current may affect the potential distribution in the conductive surface layer. In order to estimate the influence of the substrate current, we performed numerical calculations of the potential profile and found that in the case of our

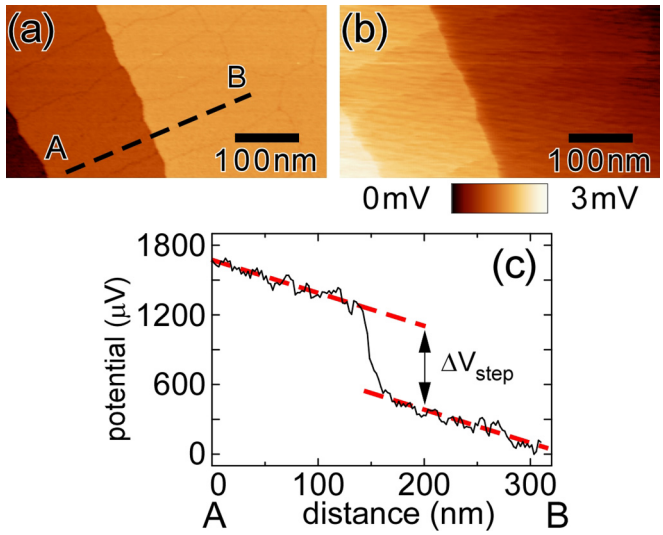

FIG. 2. STM (a) and potential (b) images taken simultaneously in the area that includes a bilayer-height step on the Si(111)-7 × 7 surface. The applied voltage and net current flowing through the Ta pads are 7.8 V and 1.29 mA, respectively. (c) Cross-sectional plot along the line A-B, which is depicted with a dashed line in panel (a).

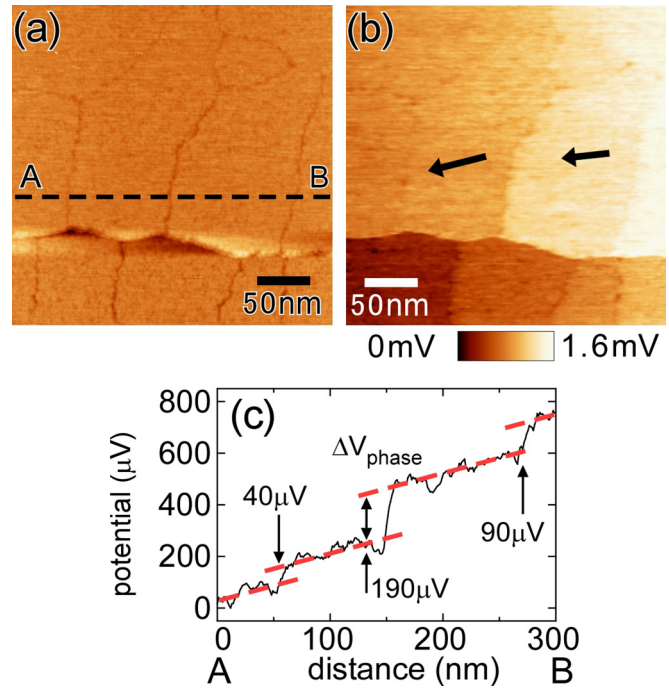

FIG. 3. STM (a) and potential (b) images taken simultaneously in the area that includes a bilayer-height step and several phase boundaries on the Si(111)-7 × 7 surface. The arrows drawn in the potential image (b) indicate the direction of current in the domains measured from the gradient of the potential. The applied voltage and net current flowing through the Ta pads are 7.8 V and 1.3 mA, respectively. (c) Cross-sectional plot along the line A-B, which is depicted with a dashed line in panel (a).

low-doped sample the ratio is not affected by the conductance through the substrate, as discussed in detail in Supplemental Material [31]. The low-doped substrate safely eliminates the problem of the bulk contributions, which otherwise requires additional procedures such as conductance measurements under molecular adsorption or probe-spacing dependent measurements in the analysis of the surface conductivity by STP and macroscopic methods [10,12].

Using the formula, we first estimated the conductivity ratio σ_s/σ_t of a single step to the terrace of the Si(111)-7 × 7 surface from the data shown in Fig. 2. The cross-sectional potential profile across a single bilayer-high step was taken normal to the step edge. When the potential profile is measured in the perpendicular direction to the step edge ($\theta = \varphi$), the two cosine terms in the equation are canceled out. The ratio can thus be simply obtained as $\sigma_s/\sigma_t = E/\Delta V_{\text{step}}$ regardless of the local current direction. For the estimation of E we adopted an average of the potential gradient measured in both sides of the step. From potential profiles like the one shown in Fig. 2(c), we found that the ratio σ_s/σ_t is 3.1 ± 1 /μm. The obtained value is consistent with those reported in previous works [10,12].

The local miscut angle of the substrate from the nominal (111) plane, estimated from the step density in the STM images, is as small as $\sim0.3^\circ$, within tolerance of the miscut angle of commercially available Si wafers ($<0.5^\circ$). Even on nominally (111)-oriented substrates the step resistance has a significant influence on the current distribution [10,12]. The ratio means that the resistance of a single step corresponds to that of the 340-nm-width terrace of the 7 × 7 structure, indicating that the contribution of the steps to the net resistance dominates when the tilting angle exceeds 0.06°. The macroscopically measured total resistance through the 7 × 7 surface states is therefore basically determined by the step density and local misoriented angle. Since the step-dominant critical angle, 0.06°, is much smaller than the tolerance of the miscut angle, one basically cannot control the step density and the net surface conductivity. This explains the large variation in the reported values of macroscopic surface conductance measurements.

B. Conductivity across a domain boundary

We then measured the conductivity ratio of a single phase boundary to the terrace σ_{pb}/σ_t of the Si(111)-7 × 7 surface from the data shown in Fig. 3. As the resistivity of the phase boundary is smaller than the steps, the amount of the potential drop is also small. In order to avoid influence of the thermal drift in the potential measurement, we analyzed a potential profile measured along the scanning (horizontal) direction. The amount and direction of the potential gradient E were obtained from a plane fitting of the whole terrace. From the values of E, ΔV, θ, and φ measured at several sites we estimated the conductivity ratio σ_{pb}/σ_t as $(16.4 \pm 10)/\mu$m. The considerable variation in the estimated value could be due to the dependence of the conductance on the type of domain boundaries, and further measurements are needed to confirm this speculation.

The ratio indicates that the phase boundary is more conductive than the step edge by a factor of ~6 on average, but has a significant resistance to cross it. The amount of the ratio means that the resistance of a single phase boundary corresponds to that of the 60-nm-width terrace. In the case of the sample examined in Fig. 3, phase boundaries exist with

the density of around 1 per 100 nm, and the resistance of the phase boundaries contributes 38% of the total resistance along the step edge direction.

The distribution of phase domains of the 7×7 structure and their size are closely related with the nucleation process of the 7×7 structure from a disordered 1×1 structure during the cooling of the sample after the 1200 °C annealing. The 7×7 domains nucleate at the upper side edge of steps with a triangular shape surrounded by the faulted halves. The size of the 7×7 phase domains, that is, the separation of the phase domain boundaries, depends on local step orientation and separation [33,34]. In the wide step separation and slow cooling, the domain size is limited by the built-in strain induced by the 7×7 formation [33,34]. According to the studies by Hibino and Ogino [33] and Hibino [34], the domain size is limited in the range of 300 to 700 nm depending on the step orientation, quite large compared with ours, presumably due to difference in the cooling process. This also indicates that the macroscopic surface conductivity depends on the sample preparation methods.

Using four probes arranged in a square form [10,11,35], the step and terrace conductivities have been estimated through the anisotropy of conductance along and across steps. In the analysis, the resistance measured along steps is assumed to be that of terraces whereas the one measured across steps includes the resistance of both steps and terraces. The significant contribution of the domain boundary, as revealed in our present paper, implies that the estimation of the conductivity of the 7×7 terrace based on the conductance anisotropy should be performed with care; the terrace conductivity is underestimated when the resistance of domain boundaries is neglected. The results indicate that, in order to estimate the intrinsic conductance, microscopic characterization is obviously needed.

In conclusion, by operating STP in UHV conditions, we have quantitatively measured the electrical conductivity ratio of a single step and domain boundary to the terrace on the Si(111)-7×7 surface. The resistivity of the domain boundary is smaller than that of the steps, but still has a significant contribution to the net conductance along the step edges. Our presented results clearly demonstrate the importance of characterizing microscopic conductance to elucidate the intrinsic transport properties of the metallic surface states.

ACKNOWLEDGMENTS

We acknowledge Hiroki Hibino for fruitful discussion. This work is partially supported by Grants-in-Aid for Scientific Research (Grants No. 16K04956, No. 16H02109, and No. 18K19013) from the Ministry of Education, Culture, Sports, Science, and Technology of Japan.

[1] K. S. Novoselov, A. K. Geim, S. V. Morozov, D. Jiang, Y. Zhang, S. V. Dubonos, I. V. Grigorieva, and A. A. Firsov, Science **306**, 666 (2004).
[2] Q. H. Wang, K. Kalantar-Zadeh, A. Kis, J. N. Coleman, and M. S. Strano, Nat. Nanotech. **7**, 699 (2012).
[3] M. Chhowalla, H. S. Shin, G. Eda, L. J. Li, K. P. Loh, and H. Zhang, Nat. Chem. **5**, 263 (2013).
[4] S. Hasegawa and S. Ino, Phys. Rev. Lett. **68**, 1192 (1992).
[5] Y. Nakajima, S. Takeda, T. Nagao, S. Hasegawa, and X. Tong, Phys. Rev. B **56**, 6782 (1997).
[6] F. Ming, S. Johnston, D. Mulugeta, T. S. Smith, P. Vilmercati, G. Lee, T. A. Maier, P. C. Snijders, and H. H. Weitering, Phys. Rev. Lett. **119**, 266802 (2017).
[7] T. Zhang, P. Cheng, W.-J. Li, Y.-J. Sun, G. Wang, X.-G. Zhu, K. He, L. Wang, X. Ma, Xi Chen, Y. Wang, Y. Liu, H.-Q. Lin, J.-F. Jia, and Q.-K. Xue, Nat. Phys. **6**, 104 (2010).
[8] S. Hasegawa, I. Shiraki, F. Tanabe, and R. Hobara, Curr. Appl. Phys. **2**465 (2002).
[9] S. Hasegawa, I. Shiraki, F. Tanabe, R. Hobara, T. Kanagawa, T. Tanikawa, and I. Matsuda, Surf. Rev. Lett. **10**, 963 (2003).
[10] S. Just, M. Blab, S. Korte, V. Cherepanov, H. Soltner, and B. Voigtländer, Phys. Rev. Lett. **115**, 066801 (2015).
[11] I. Matsuda, M. Ueno, T. Hirahara, R. Hobara, H. Morikawa, C. Liu, and S. Hasegawa, Phys. Rev. Lett. **93**, 236801 (2004).
[12] B. V. C. Martins, M. Smeu, L. Livadaru, H. Guo, and R. A. Wolkow, Phys. Rev. Lett. **112**, 246802 (2014).
[13] S. Heike, S. Watanabe, Y. Wada, and T. Hashizume, Phys. Rev. Lett. **81**, 890 (1998).
[14] J. Homoth, M. Wenderoth, T. Druga, L. Winking, R. G. Ulbrich, C. A. Bobisch, B. Weyers, A. Bannani, E. Zubkov, A. M. Bernhart, M. R. Kaspers, and R. Möller, Nano Lett. **9**, 1588 (2009).
[15] F. Lüpke, S. Korte, V. Cherepanov, and B. Voigtländer, Rev. Sci. Instrum. **86**, 123701 (2015).
[16] T. Uchihashi, P. Mishra, M. Aono, and T. Nakayama, Phys. Rev. Lett. **107**, 207001 (2011).
[17] T. Nakamura, R. Yoshino, R. Hobara, S. Hasegawa, and T. Hirahara, e-J. Surf. Sci. Nanotech. **14**, 216 (2016).
[18] Y. Hasegawa, I.-W. Lyo, and Ph. Avouris, Surf. Sci. **357**, 32 (1996).
[19] K. Yoo and H. H. Weitering, Phys. Rev. B **65**, 115424 (2002).
[20] T. Tanikawa, K. Yoo, I. Matsuda, S. Hasegawa, and Y. Hasegawa, Phys. Rev. B **68**, 113303 (2003).
[21] M. D'angelo, K. Takase, N. Miyata, T. Hirahara, S. Hasegawa, A. Nishide, M. Ogawa, and I. Matsuda, Phys. Rev. B **79**, 035318 (2009).
[22] J. W. Wells, J. F. Kallehauge, T. M. Hansen, and Ph. Hofmann, Phys. Rev. Lett. **97**, 206803 (2006).
[23] P. Muralt and D. W. Pohl, Appl. Phys. Lett. **48**, 514 (1986).
[24] M. Rozler and M. R. Beasley, Rev. Sci. Instrum. **79**, 073904 (2008).
[25] A. Bannania, C. A. Bobischb, and R. Möller, Rev. Sci. Instrum. **79**, 083704 (2008).
[26] T. Druga, M. Wenderoth, J. Homoth, M. A. Schneider, and R. G. Ulbrich, Rev. Sci. Instrum. **81**, 083704 (2010).
[27] S.-H. Ji, J. B. Hannon, R. M. Tromp, V. Perebeinos, J. Tersoff, and F. M. Ross, Nat Mater. **11**, 114 (2012).
[28] M. Hamada and Y. Hasegawa, Jpn. J. Appl. Phys. **51**, 125202 (2012).

[29] P. Willke, T. Druga, R. G. Ulbrich, M. A. Schneider, and M. Wenderoth, Nat. Commun. **6**, 6399 (2015).
[30] K. W. Clark, X.-G. Zhang, I. V. Vlassiouk, G. He, R. M. Feenstra, and An-Ping Li, ACS Nano. **7**, 7956 (2013).
[31] See Supplemental Material at http://link.aps.org/supplemental/10.1103/PhysRevB.99.125402 for numerical calculations of the potential profile, which includes Ref. [32].
[32] F. J. Himpsel, G. Hollinger, and R. A. Pollak, Phys. Rev. B **28**, 7014 (1983).
[33] H. Hibino and T. Ogino, Appl. Phys. Lett. **67**, 915 (1995).
[34] H. Hibino, Ph.D. thesis, Waseda University, 2006.
[35] T. Kanagawa, R. Hobara, I. Matsuda, T. Tanikawa, A. Natori, and S. Hasegawa, Phys. Rev. Lett. **91**, 036805 (2003).